

Flexible Color-Tunable Electroluminescent Devices by Designing Dielectric-Distinguishing Double-Stacked Emissive Layers

Yong Zuo, Xiang Shi, Xufeng Zhou, Xiaojie Xu, Jun Wang, Peining Chen, Xuemei Sun,* and Huisheng Peng*

Intrinsically flexible alternating current electroluminescent devices have sparked widespread research interest due to their tremendous potential in bioinspired electronics, smart wearables, and human–machine interfaces. In these applications, it is highly desirable to possess real-time color tunability but this has not been reported yet. Herein, a flexible color-tunable electroluminescent device composed of simple double-stacked emissive layers of ZnS phosphors/dielectric polymer composite is developed by an all-solution processable method. The color tuning capability can be attributed to the dielectric difference between the two emissive layers, leading to the color combination between two independent emissions originating from different ZnS phosphors at varied electric fields. With the rational selection of the dielectric polymer matrices, a wide-range color tuning from orange to white and to blue can be realized in a single device just by varying the electric field. It also exhibits high mechanical robustness with well-maintained performance even after 1000 cycles of bending. Similar natural functionalities like camouflage and visual communication can be further reproduced in the artificial color-tunable system, thereby opening a general and effective avenue for developing smart wearables and soft electronics.

1. Introduction

In nature, abundant functionalities of living things have guided us to develop artificial systems that mimic similar capabilities to interact well with the environment.^[1–6] Recently, bionics has been widely applied in the construction of various electronic devices such as sensors,^[7,8] nanogenerators,^[9,10] batteries,^[11,12]

Y. Zuo, X. Shi, X. Zhou, Dr. X. Xu, Prof. P. Chen, Prof. X. Sun, Prof. H. Peng

State Key Laboratory of Molecular Engineering of Polymers
Department of Macromolecular Science, and Laboratory
of Advanced Materials

Fudan University
Shanghai 200438, China

E-mail: sunxm@fudan.edu.cn; penghs@fudan.edu.cn

Prof. J. Wang
Department of Materials Science
Fudan University
Shanghai 200438, China

 The ORCID identification number(s) for the author(s) of this article can be found under <https://doi.org/10.1002/adfm.202005200>.

DOI: 10.1002/adfm.202005200

and integrated systems.^[13–16] As an indispensable component for electronic devices and a key window of information communication, the optoelectronic display is no exception. Several electroluminescent (EL) devices, such as light-emitting diodes^[17,18] and alternating current electroluminescent (ACEL) devices,^[19–21] have been explored to reproduce some exceptional capabilities. Among these EL devices, the ACEL device with simplified structure has attractive attributes such as simple manufacturing process, excellent durability, easy integration, and stable performance in harsh environments, and thus stands out and has been extensively used in bioinspired systems.^[22–24] Many functionalities of biological systems such as ultraviolet response, self-healing, and stretching have been successfully replicated in this kind of device by introducing functional polymers and designing device architectures, demonstrating tremendous potential applications in many emerging important fields

of information encryption,^[25,26] electronic skin,^[20,27,28] and soft robots.^[19,21,29]

Moreover, color diversity and dynamic tunability of an EL device are essential for applications in display and communication. Just as numerous deep-sea fish with the ability of self-illuminate (e.g., mesopelagic squid) can change their bioluminescence color for optical signaling in order to disguise, protection, predation, or communication.^[30–32] Although some attempts have been made to realize multicolor emissions by regulating material's composition or introducing color-conversion layer,^[33–36] the ACEL device commonly used in bioinspired electronics has not gained the ability of dynamic color change yet.

Herein, we introduced a flexible ACEL device that enabled emission color tuning by changing the electric field. This function was achieved by designing dielectric-distinguishing double-stacked emissive layers. One was orange-emissive layer with low dielectric constant, while the other was blue-emissive layer with high dielectric constant. Its color could be readily tuned from orange to white and to blue as the electric field strength increased. Furthermore, the range of color tuning could be effectively enlarged by regulating the driving frequency. More

importantly, this color-tunable device exhibited an excellent flexibility and robustness, and could be designed into any pattern for camouflage and communication.

2. Results and Discussion

2.1. Structure Design and Optical Properties

Figure 1a schematically illustrates the structure of our flexible color-tunable ACEL device. The device consisted of double-stacked emissive layers that were sandwiched between flexible indium-tin oxide (ITO)/poly(ethylene terephthalate) (PET) and silver nanowires (AgNWs) electrodes. The double emissive layers were prepared by embedding different metal-doped ZnS phosphors into various flexible polymer matrices with different dielectric constants so as to induce difference of luminescent performance between the two emissive layers. As a prototype device, ZnS:Mn phosphors were dispersed into polystyrene-*b*-polybutadiene-*b*-polystyrene (SBS) to form an orange-emissive layer, and ZnS:Cu phosphors were distributed in cyanoresin (CR) to form a blue-emissive layer. The device was fabricated

using a facile solution-processed method (Figure S1, Supporting Information), which was beneficial for further large-scale production. The detailed fabrication process was shown in the Experimental Section.

The layer-by-layer stack structure of the obtained device was verified by the cross-sectional scanning electron microscopy (SEM), and the image also indicated the clear interface and close contact between two neighboring layers (Figure 1b). These results were also visualized by fluorescence microscopy (Figure 1c), revealing that ZnS:Mn and ZnS:Cu phosphors with an average diameter of $\approx 25 \mu\text{m}$ (Figures S2 and S3, Supporting Information) were uniformly distributed within the SBS and CR matrices, respectively. The thicknesses of orange and blue-emissive layers were similar of around $50 \mu\text{m}$. AgNWs were well distributed to form a conductive interconnected network as the top electrode (Figure S4, Supporting Information). Under an alternating electric field, the light was emitted from metal-doped ZnS phosphors due to the radiative relaxation of the luminescent center.^[37] When the applied electric field strength increased, a noticeable emitting color change from orange ($1 \text{ V } \mu\text{m}^{-1}$), to warm white ($2 \text{ V } \mu\text{m}^{-1}$), to cool white ($3 \text{ V } \mu\text{m}^{-1}$), and finally to blue ($5 \text{ V } \mu\text{m}^{-1}$) could be observed (Figure 1d).

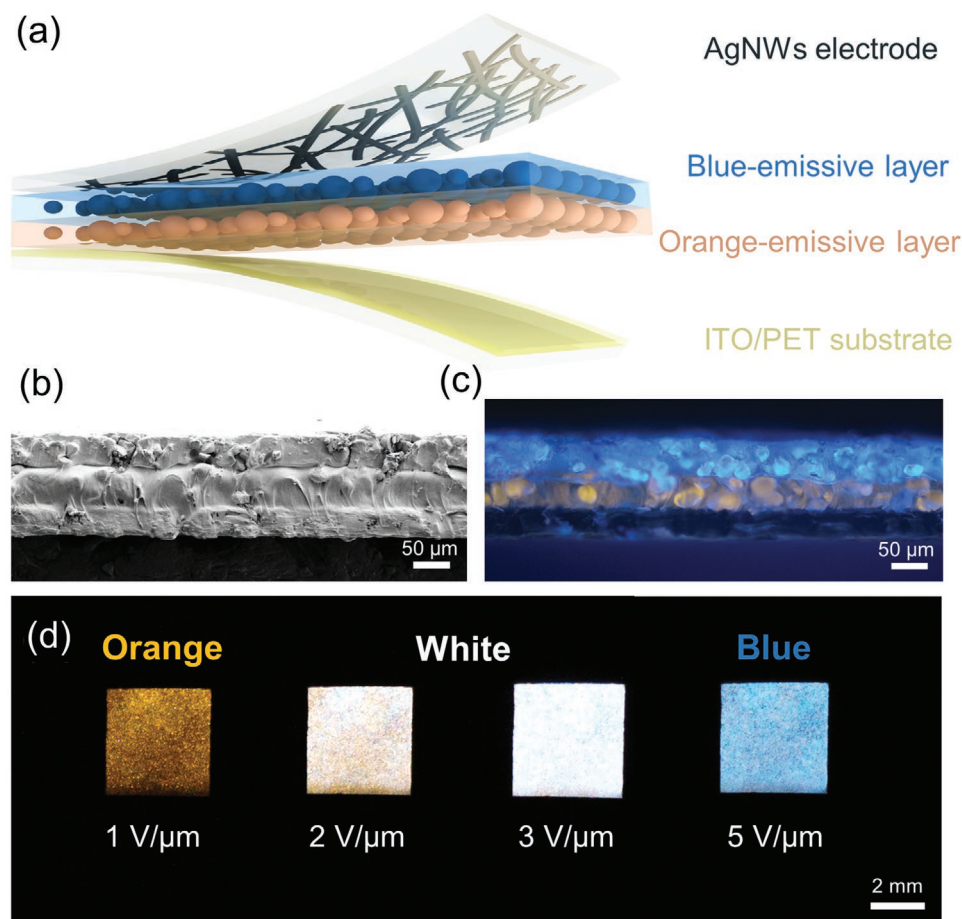


Figure 1. Structure and photographs of the color-tunable ACEL device. a) Schematic illustrating the designed flexible color-tunable ACEL device with double-stacked emissive layers between two electrodes. b) Cross-sectional SEM image and c) fluorescence image of the device. d) Photographs of the device showing color change from orange, to white and to blue at different applied electric fields.

2.2. Mechanism of Color Tuning

To shed light on the detailed color-tuning mechanism of the ACEL device with double-stacked emissive layers, a series of monochromatic ACEL devices with a single emissive layer were firstly investigated. ZnS:Mn or ZnS:Cu phosphors were incorporated into polymer matrix (SBS or CR) independently. **Figure 2a** presents the EL spectra of the monochromatic devices, illustrating ZnS:Cu and ZnS:Mn phosphors have their peak emissions at 458 and 586 nm, respectively, at the electric frequency of 2 kHz. Meanwhile, the monochromatic device comprising ZnS:Cu phosphors exhibited higher EL intensity than that one with ZnS:Mn phosphors at the same applied electric field (Figures S5a and S6a, Supporting Information) because Mn²⁺ traps holes in ZnS under the alternating electric field may deteriorate electron–hole recombination.^[38] As the electric field strength increased, the EL intensity increased rapidly, while central

peak locations remained unchanged (Figures S5b,c and S6b,c, Supporting Information). Furthermore, when ZnS:Mn and ZnS:Cu phosphors (weight ratio = 1:1) were uniformly mixed in a polymer matrix together, blue light was observed by naked eyes (Figure S7, Supporting Information) due to higher intensity of ZnS:Cu phosphors. And thus a blue band with a maximum at 458 nm originated from ZnS:Cu phosphors dominated in their EL spectra (Figure 2b and Figure S8a, Supporting Information). There was no obvious change in EL spectra and corresponding Commission Internationale de l'Éclairage (CIE) coordinates as the color balance between the two phosphors was maintained throughout the entire electric field region, illustrating that such devices with a single emissive layer containing mixed color phosphors were incapable of tuning colors (Figure 2c and Figure S8b and Table S1, Supporting Information).

As for the ACEL device with double-stacked emissive layers, it can be equivalent to two capacitors connected in series

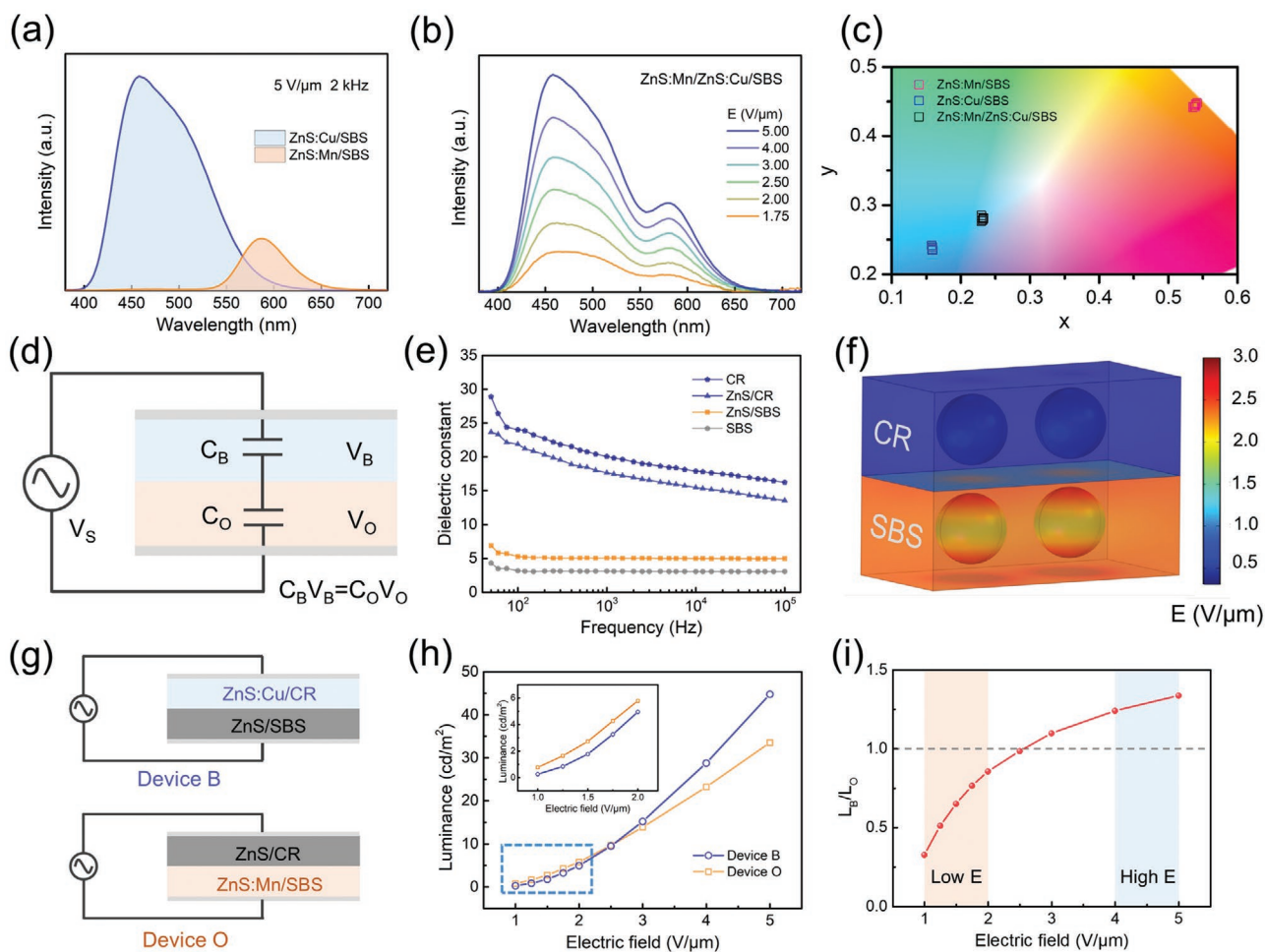


Figure 2. Working mechanism of the color-tunable ACEL device. a) EL spectra of the monochromatic ACEL devices with a single emissive layer (ZnS:Cu/SBS or ZnS:Mn/SBS) driven at $5 \text{ V } \mu\text{m}^{-1}$ and 2 kHz. b) EL spectra of the ACEL device with a single emissive layer (ZnS:Mn/ZnS:Cu/SBS) operated at varied electric fields. c) Corresponding CIE coordinates of the ACEL devices with a single emissive layer at varied electric fields. d) Equivalent circuit of the ACEL device showing two capacitors connected in series. e) Frequency-dependent dielectric constant of CR, ZnS/CR, ZnS/SBS, and SBS. f) Simulation of electric field distribution in the ACEL device with double-stacked emissive layers. g) Schematic of the structure of the analogous devices (devices B and O) with nonluminescent ZnS layer replacing ZnS emissive layer. h) Luminance as a function of electric field for devices B and O. Inset is a magnification of the blue rectangle showing their relationship at low electric field region. i) Luminance ratio (L_B/L_O) as a function of electric field. L_B and L_O represent the luminance of Device B and O, respectively.

according to its EL mechanism,^[39] as shown in Figure 2d. Capacitors C_B and C_O were formed by ZnS:Cu/CR and ZnS:Mn/SBS emissive layers, respectively. Assume that an alternating voltage (V_s) is applied to the device, the charges stored in each capacitor are the same, and thus the distributed voltage follows the relation

$$C_B V_B = C_O V_O \quad (1)$$

where V_B and V_O are, respectively, the distributed voltage in the blue and orange-emissive layers.

According to previous reports, the EL properties directly depend on the electric field focused on the ZnS emissive layer.^[21,40–42] Furthermore, the capacitance distribution within the double emissive layers is governed by the dielectric properties of each layer. As is well known, the dielectric constant (ϵ) and electric field (E) can be expressed by the following equations

$$\epsilon = 4\pi k d C / S \quad (2)$$

$$E = V / d \quad (3)$$

where k , S , and d are electrostatic force constant, facing area between the two electrodes, and vertical distance between the two electrodes, respectively. Therefore, it is not hard to obtain the relationship between electric field and dielectric constant of each layer in ACEL device with double-stacked emissive layers, namely

$$\epsilon_B E_B = \epsilon_O E_O \quad (4)$$

As shown in Figure 2e, the measured frequency-dielectric constant curves indicate that the dielectric constant of CR was much higher than that of SBS in the entire frequency range. After mixing ZnS phosphors, the dielectric constant of the ZnS/CR composite was still higher than that of ZnS/SBS composite. For example, ZnS/CR composite showed a high dielectric constant of 16.9 at the frequency of 2 kHz, which was 3-fold higher than ZnS/SBS composite. That is to say, the dielectric constant of blue-emissive layer (ϵ_B) was higher than the orange one (ϵ_O) in our ACEL device. Therefore, according to Equation (4), the electric field strength distributed in blue-emissive layer (E_B) was lower than the orange one (E_O). The simulation results of the electric field distribution also confirmed that more electric field was concentrated on the orange-emissive layer with a lower dielectric constant (Figure 2f and Figure S9, Supporting Information), thereby easily to excite ZnS:Mn phosphors to produce orange emission upon applying an electric field. We can infer that when the alternating voltage increased, the electric field distributed on the blue-emissive layer rose accordingly and became strong enough to excite ZnS:Cu phosphors to emit blue light, leading to white light emission from a mixture of those two lights. A further increase in strength of the electric field was accompanied by an increase of the EL intensity, and the blue emission dominated at higher electric field region arising from the EL property difference between the two phosphors discussed above.

To clarify the mechanism behind the color tunability of the double-emission-layers device, as shown in Figure 2g, ZnS:Mn

and ZnS:Cu phosphors were replaced by nonluminous ZnS particles, respectively, to fabricate analogous devices (devices B and O) so as to investigate the characteristics of a single emissive layer. As can be seen from their EL spectra and corresponding CIE coordinates at various electric fields (Figure S10, Supporting Information), both devices exhibited monochromatic emission without color change. With regard to luminance values at different electric fields (Figure 2h), the luminance of Device O was higher than that of Device B at low electric fields ($<2 \text{ V } \mu\text{m}^{-1}$); when the electric field strength increased, the difference in luminance between these two devices was narrowed, i.e., their luminance ratio (L_B/L_O) was close to 1 (Figure 2i). In the high electric field range ($>4 \text{ V } \mu\text{m}^{-1}$), the luminance of Device B exceeded that of Device O, and the ratio increased to over 1. These results thus exactly confirmed our above-mentioned conjecture and perfectly explained the color change from orange to white and to blue as the electric field strength increased.

In addition, when the double emissive layers were changed into ZnS:Cu/SBS and ZnS:Mn/CR composites, only blue light can be observed (Figure S11, Supporting Information). In this case, higher electric field was distributed in blue-emissive layer with low dielectric constant (ZnS:Cu/SBS), providing no chance for ZnS:Mn phosphors to emit enough orange light to catch up and exceed the blue light due to lower EL intensity, and thus the intensity of blue-emissive layer always exceeded that of orange one at varied electric fields. Therefore, in order to achieve color-tunable emission, ZnS:Cu phosphors with higher EL intensity should be combined with high dielectric polymer and ZnS:Mn phosphors with lower intensity should be mixed with low dielectric polymer.

2.3. Color-Tuning Performance

Figure 3a presents the EL spectra of the color-tunable ACEL device operated at various electric fields. It is clear that orange emission originated from ZnS:Mn phosphors was dominant at low electric fields, whereas blue emission from ZnS:Cu phosphors increased with continuously increasing electric field strength, and finally the blue emission became strong enough to dominate the overall EL spectra. The similar trends of color tuning were also found by changing the content of ZnS:Cu phosphors from 30% to 70% and the blue emission was dominant at lower electric fields as the content increased due to the higher intensity of the blue-emissive layer with the growing luminescent phosphors (Figure S12 and Table S2, Supporting Information).

To further verify it is the difference in dielectric properties of two emissive layers that contributed to the color tuning, other flexible dielectric polymer materials (Figure S13, Supporting Information), such as poly(vinylidene fluoride-co-hexafluoropropylene) (PVDF-HFP) ($\epsilon = 11.6$, 2 kHz) and polyurethane (PU) ($\epsilon = 6.8$, 2 kHz) and SBS ($\epsilon = 3.1$, 2 kHz), have been utilized as polymer matrices in blue-emissive layer, and their detailed EL performances were provided in Figure S14 (Supporting Information). Since the intensity difference in the two emissive layers directly determined the color change, the relationship between electric field and the ratio of I_{458}/I_{586} (I_{458} and I_{586} are the emission peak

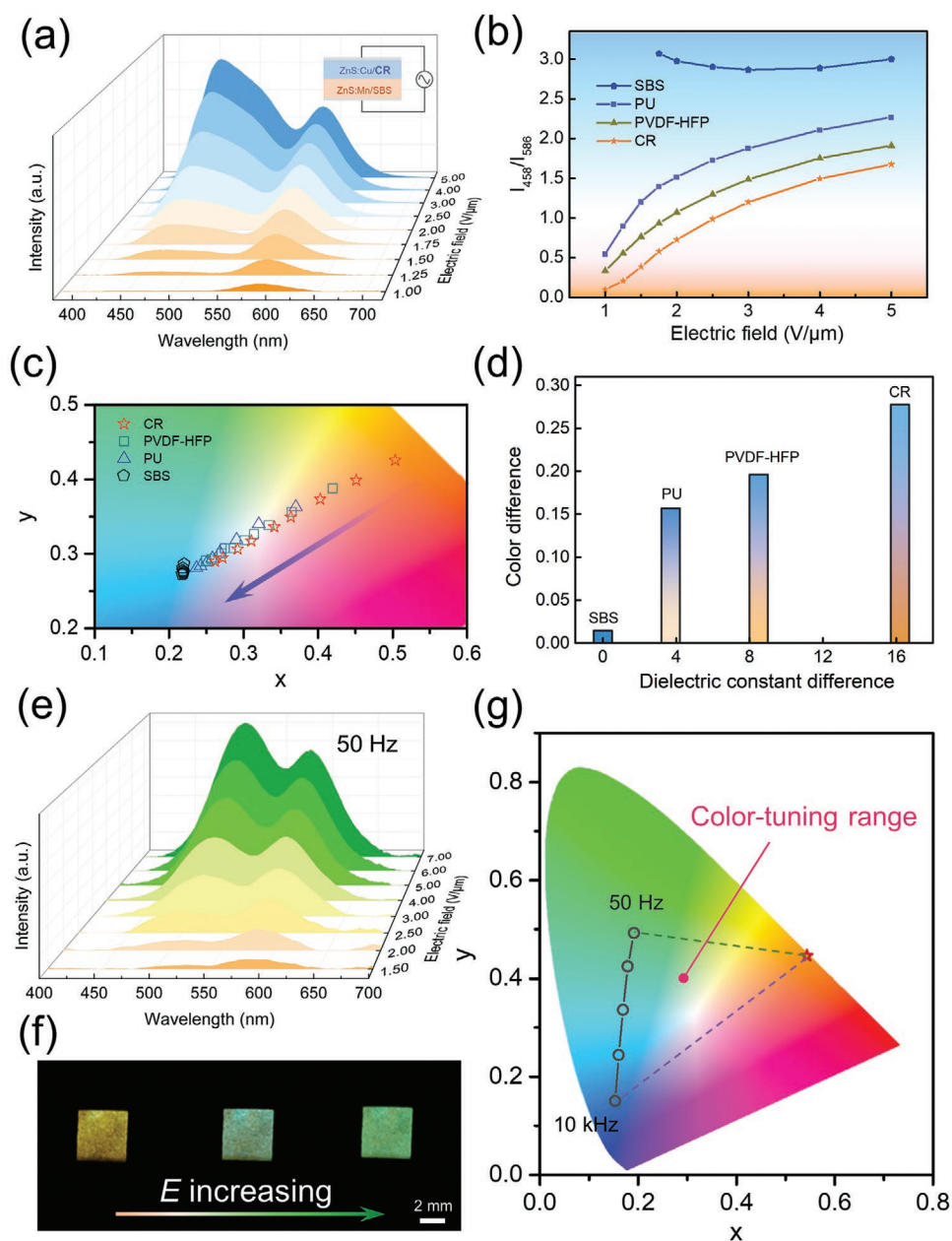


Figure 3. Color-tuning performance of the color-tunable ACEL device. a) EL spectra of the ACEL device using CR as polymer matrix in blue-emissive layer operated at varied electric fields and at the frequency of 2 kHz. b) I_{458}/I_{586} value and c) corresponding CIE coordinates of the ACEL devices with different polymer matrices in blue-emissive layer at varied electric fields. d) Relationship between color difference and dielectric constant difference. e) EL spectra and f) photographs of the ACEL device using CR as polymer matrix in blue-emissive layer operated at varied electric fields and at the frequency of 50 Hz. g) Possible color-tuning range (triangle) of the single color-tunable ACEL device.

intensities at 458 and 586 nm, respectively) was carefully analyzed (Figure 3b). I_{458}/I_{586} showed similar trends with increasing electric fields among the devices employing CR, PVDF-HFP, and PU. Unlike the CR-contained device, PVDF-HFP and PU based devices showed almost no orange emission because the blue-emission peak intensity exceeded the orange-emission one at a lower electric field strength. Accordingly, the CIE coordinates varied from (0.5035, 0.4254) to (0.2618, 0.2894) by increasing electric field from 1 to 5 $V \mu m^{-1}$ for CR-contained device (Figure 3c and Table S3, Supporting Information). When PU was used as

polymer matrix in blue-emissive layer, a slight color change from (0.3700, 0.3629) to white (0.2368, 0.2806) can be observed within the same measured range of the electric field. It can be attributed to the relatively low electric field difference between orange-emissive layer and blue-emissive layer resulting from low dielectric constant difference, which thus allowed both emissive layers to emit light at low applied electric fields (Figure S15, Supporting Information). Due to the same dielectric constant in both emissive layers, the emitting color of the device with SBS-contained blue-emissive layer was blue, no color change (CIE coordinates

around (0.22, 0.27) appeared as the electric field increased, and I_{458}/I_{586} remained at around 3, which is similar to the device with single emissive layer (ZnS:Mn/ZnS:Cu/SBS).

Color difference (CD) can be generally expressed by the Euclidean distance between two points (x_1, y_1) and (x_2, y_2) in the CIE diagram to quantitatively evaluate the color-tuning range,^[43] and it is calculated by

$$CD = \sqrt{(x_1 - x_2)^2 + (y_1 - y_2)^2} \quad (5)$$

Figure 3d shows the relationship between the color difference and the dielectric constant difference from two dielectric polymer matrices, indicating that the larger the difference between the dielectric constants of the two emissive layers, the wider the range of color tuning. A wider color change may be obtained by further developing polymer matrix with higher dielectric constant or introducing high dielectric particles like BaTiO₃ to the blue-emissive layer.^[40–42]

Interestingly, ZnS:Cu phosphors exhibited color change from blue to green emissions as the driving frequency decreased due to different trapping states formed by Cu doping,^[44,45] whereas the ZnS:Mn phosphors maintained unchanged (Figure S16, Supporting Information). This result provided the possibility for

emitting other colors in our ACEL device and thus expanding the color-tuning range. Figure 3e,f presents the color change behavior under various electric fields at the frequency of 50 Hz. In this case, orange emission was dominant at low electric field, whereas the intensity of green emission centered at 510 nm relative to orange emission gradually increased when the electric field was strengthened continually (Figure 3e). An obvious color change from orange to green was detected by the naked eyes (Figure 3f), and corresponding CIE coordinates shifted from (0.4803, 0.3626) to (0.3314, 0.4734) (Figure S17, Supporting Information). Based on these results, we can conclude that the dynamic color-tuning range of our single ACEL device forms a triangle as depicted in the CIE diagram (Figure 3g). Any color within the triangle can be displayed with a specific driving electric field and frequency. Other colors like red may be obtained by further introducing fluorescent dyes.^[33,35,46]

2.4. Mechanical Flexibility and Stability

Our color-tunable ACEL device exhibited excellent mechanical flexibility and stability, evaluated by bending tests. As shown in Figure 4a, the luminescent intensity of the flexible ACEL device

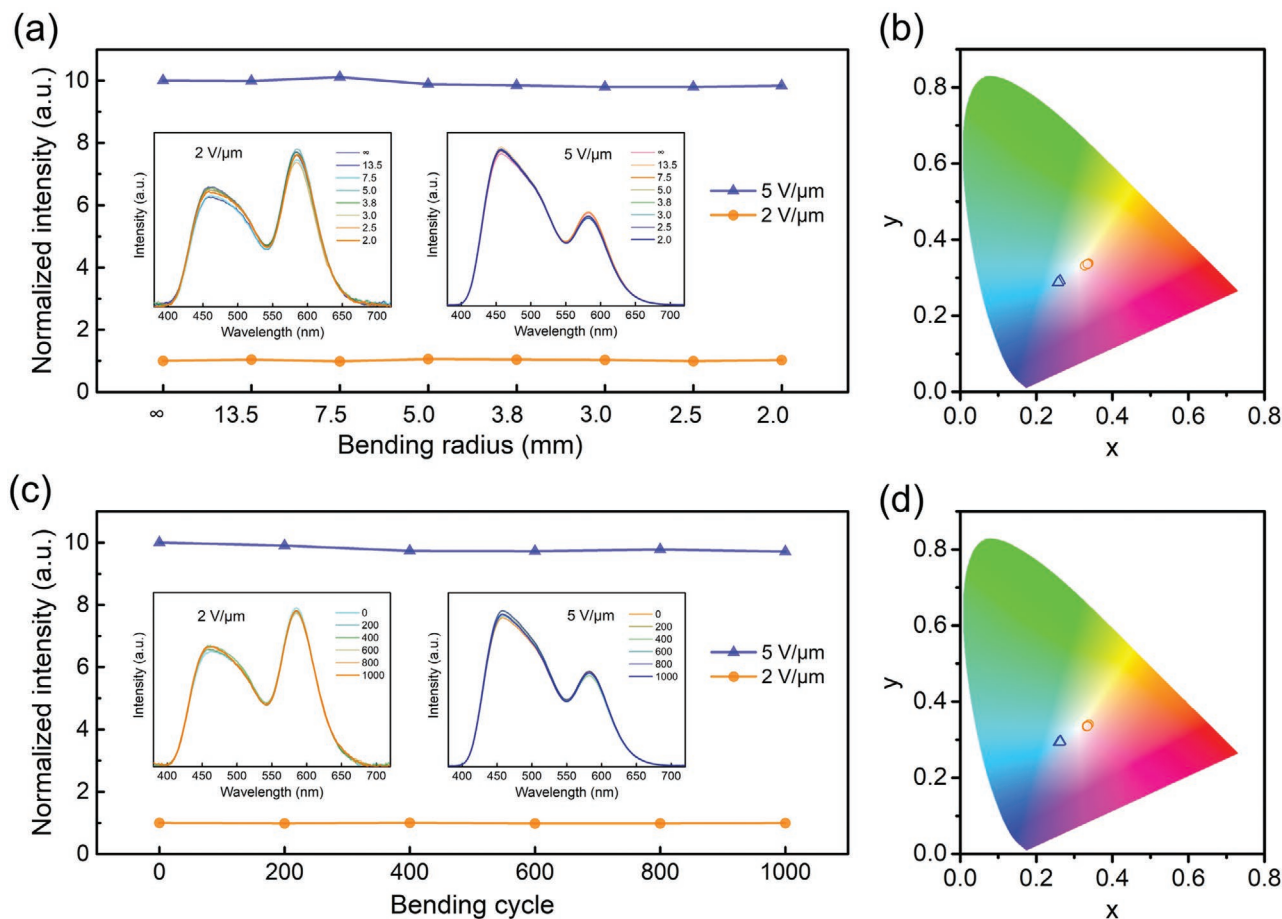


Figure 4. Flexibility and stability of the color-tunable ACEL device. a) Normalized intensity (insets, EL spectra) and b) corresponding CIE coordinates of the ACEL device under different bending radii at electric fields of 2 and 5 V μm⁻¹. c) Normalized intensity (insets, EL spectra) and d) corresponding CIE coordinates of the ACEL device with different bending cycles at electric fields of 2 and 5 V μm⁻¹ under a bending radius of 3.8 mm.

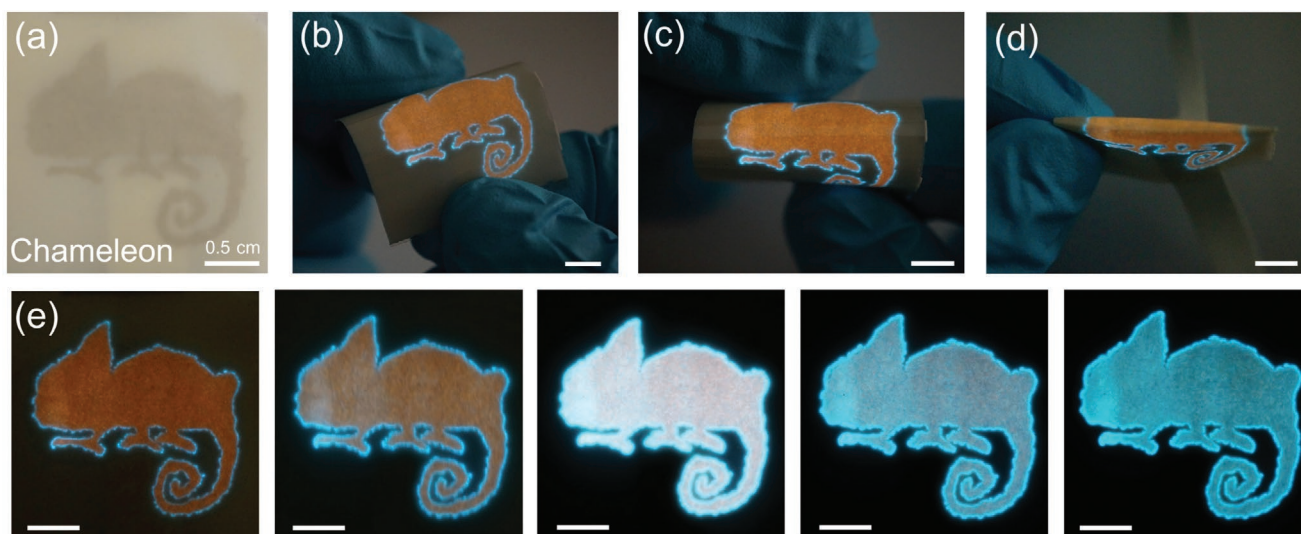


Figure 5. The ACEL device based mechanically robust “chameleon”. a) Photograph of the as-fabricated “chameleon”. b–d) Photographs of the “chameleon” under various deformed conditions. e) Real-time color change of the “chameleon” with increasing electric fields from 1 to 7 V μm^{-1} .

maintained 98% of its initial value as the bending radius was reduced, whether it was driven at the low electric field of 2 V μm^{-1} or the high electric field of 5 V μm^{-1} . Their EL spectra along with corresponding CIE coordinates kept unchanged and overlapped at various bending radii (Figure 4b and Table S4, Supporting Information), suggesting that the device remained stable during the mechanical bending process. Meanwhile, the bending durability was also investigated at a radius of 3.8 mm. The flexible ACEL device retained above 97% of their initial luminance after bending for 1000 cycles (Figure 4c). There was also no significant change in the EL spectra and CIE coordinates (Figure 4d and Table S5, Supporting Information). The device maintained white light emission (0.33, 0.33) at the electric field of 2 V μm^{-1} , and the light emitted from the device was always blue (0.26, 0.29) at the electric field of 5 V μm^{-1} . The remarkable robustness and stability of the ACEL devices can be attributed to the intrinsically flexible component of polymer matrices, enabling them the reliability for practical applications.

Inspired by nature, the dynamic color change can serve as a disguise applicable to environment or function as a signal to communicate.^[47–50] The chameleon is a good example of disguising itself by changing skin color to match its surroundings. Benefiting from all-solution processable technique, the color-tunable ACEL device can be produced at a large scale. Herein, a sample with a size of 3 cm \times 3 cm was easily fabricated via a layer-by-layer blade-coating process on the ITO/PET substrate. **Figure 5a** exhibits a flexible ACEL device with a chameleon patterned electrode. Upon applying an electric field at the frequency of 2 kHz, a bright “chameleon” appears and it can display stably under various deformed conditions and even the completely folded condition (Figure 5b–d). The “chameleon” was capable of changing color actively by adjusting the applied electric fields from 1 to 7 V μm^{-1} (Figure 5e and Movie S1, Supporting Information), which demonstrated its enormous application potential in color adjustable wearables for camouflage or fashion and in soft electronics for optical signaling.

3. Conclusion

In summary, a flexible color-tunable electroluminescent device was developed based on double-stacked emissive layers with different dielectric properties. This single device could emit various colors (e.g., orange, white, blue, and green) dynamically by regulating the driving electric field and frequency. The mechanism of the color tuning was investigated and explained by the dielectric difference between the two emissive layers, thus resulting in the combination between two independent light sources originated from the ZnS:Mn and ZnS:Cu phosphors at different electric fields. The color-tunable ACEL device demonstrated fairly stable luminescent performance under extreme bending conditions and 1000 repetitive bending cycles. It could be utilized to realize the functions of disguise and communication, providing new opportunities for the development of wearable electronics, smart robotics and human–machine interaction.

4. Experimental Section

Preparation of Different Emissive Composites: SBS (Sigma-Aldrich) was initially dissolved in toluene (Sinopharm) and then fully mixed with ZnS:Mn phosphors (Shanghai Keyan Phosphor Technology Co., Ltd.) at a weight ratio of 1:1 to prepare orange-emissive composite. Similarly, to obtain various blue-emissive composites, ZnS:Cu phosphors at 50 wt% were evenly dispersed into CR solution (Nanjing Collaborative Innovation Light Source Co., Ltd.), PVDF-HFP/dimethylformamide solution (Sigma-Aldrich/Sinopharm), waterborne PU (U-9, Shanghai Sisheng Polymer Materials Co., Ltd.), and SBS/toluene solution.

Fabrication of Flexible Devices: The orange-emissive composite was firstly spin-coated onto cleaned ITO/PET substrate (sheet resistance = 100 Ω sq^{-1} , South China Science & Technology Co., Ltd.) at 1500 rpm for 60 s to obtain a layer of \approx 50 μm thick. After the solvent was evaporated at room temperature, the blue-emissive layer was also formed by spin coating onto the orange-emissive layer, followed by drying at 100 $^{\circ}\text{C}$ for 2 h, to yield the same thickness. Finally, AgNW solution (Suzhou ColdStones Technology Co., Ltd.) was spun at a rate of 800 rpm for

60 s to form the top electrode (Figure S1, Supporting Information). The devices for experiment can be obtained after drying.

Fabrication of the “Chameleon”: Instead of spin-coating, ZnS:Mn/SBS and ZnS:Cu/CR composites were blade-coated on the surface of ITO/PET substrate with a size of 3 cm × 3 cm layer by layer and thermally cured at 100 °C for 2 h. A chameleon-shaped electrode was fabricated by coating silver paste (Uninwell International Co., Ltd.) on the emissive layer through the designed mask pattern to obtain the chameleon sample.

Characterization: The morphologies of ZnS phosphors and the devices were collected from a field emission scanning electron microscope (S-4800, Hitachi), operated at 1 kV. The cross-sectional geometry of the device was investigated by a fluorescence microscope (BX51, Olympus). The photographs were captured by a digital camera (α6000, Sony). The dielectric constants were calculated from measured capacitances on an LCR meter (TH2830, Tonghui) at different frequencies. The luminescent properties (luminance, luminescent spectrum, and CIE coordinates) of the devices were measured with a spectroradiometer (PR680, Photoresearch) under an alternating voltage supplied by a function waveform generator (33500B, Keysight) connected with a high voltage amplifier (610 E, Trek).

Simulation of the Electric Field Distribution: The model was built with finite element software COMSOL to simulate the electric field distribution of device with double-stacked emissive layers. In the 3D model, ZnS:Mn and ZnS:Cu phosphors, simplified as spheres with diameters of 25 μm, were uniformly distributed in different polymers.

Supporting Information

Supporting Information is available from the Wiley Online Library or from the author.

Acknowledgements

This work was supported by MOST (2016YFA0203302), NSFC (21634003, 51673043, 21805044), STCSM (17QA1400400, 19QA1400800), SHMEC (2017-01-07-00-07-E00062), and Yanchang Petroleum Group. The authors really appreciated the help from Xin Tao with the simulation of electric field distribution.

Conflict of Interest

The authors declare no conflict of interest.

Keywords

electroluminescent devices, color changes, double-stacked emissive layers

Received: June 19, 2020

Revised: July 31, 2020

Published online: September 13, 2020

- [1] T. Sun, L. Feng, X. Gao, L. Jiang, *Acc. Chem. Res.* **2005**, *38*, 644.
 [2] S. A. Morin, R. F. Shepherd, S. W. Kwok, A. A. Stokes, A. Nemiroski, G. M. Whitesides, *Science* **2012**, *337*, 828.
 [3] A. V. Singh, A. Rahman, N. V. G. Sudhir Kumar, A. S. Aditi, M. Galluzzi, S. Bovio, S. Barozzi, E. Montani, D. Parazzoli, *Mater. Des.* **2012**, *36*, 829.

- [4] S. Baik, H. J. Lee, D. W. Kim, J. W. Kim, Y. Lee, C. Pang, *Adv. Mater.* **2019**, *31*, 1803309.
 [5] Y. Liu, K. He, G. Chen, W. R. Leow, X. Chen, *Chem. Rev.* **2017**, *117*, 12893.
 [6] S. Babae, S. Pajovic, A. Rafsanjani, Y. Shi, K. Bertoldi, G. Traverso, *Nat. Biomed. Eng.* **2020**, *4*, 778.
 [7] M. Valle, *Sensors* **2011**, *11*, 10180.
 [8] H.-H. Chou, A. Nguyen, A. Chortos, J. W. F. To, C. Lu, J. Mei, T. Kurosawa, W.-G. Bae, J. B. H. Tok, Z. Bao, *Nat. Commun.* **2015**, *6*, 8011.
 [9] D.-M. Shin, H. J. Han, W.-G. Kim, E. Kim, C. Kim, S. W. Hong, H. K. Kim, J.-W. Oh, Y.-H. Hwang, *Energy Environ. Sci.* **2015**, *8*, 3198.
 [10] G. Yao, L. Xu, X. Cheng, Y. Li, X. Huang, W. Guo, S. Liu, Z. L. Wang, H. Wu, *Adv. Funct. Mater.* **2020**, *30*, 1907312.
 [11] G. Zhou, Y. E. Miao, Z. Wei, L. L. Mo, F. Lai, Y. Wu, J. Ma, T. Liu, *Adv. Funct. Mater.* **2018**, *28*, 1804629.
 [12] G. Qian, B. Zhu, X. Liao, H. Zhai, A. Srinivasan, N. J. Fritz, Q. Cheng, M. Ning, B. Qie, Y. Li, S. Yuan, J. Zhu, X. Chen, Y. Yang, *Adv. Mater.* **2018**, *30*, 1704947.
 [13] C. Zhang, W. Bin Ye, K. Zhou, H. Y. Chen, J. Q. Yang, G. Ding, X. Chen, Y. Zhou, L. Zhou, F. Li, S. T. Han, *Adv. Funct. Mater.* **2019**, *29*, 1808783.
 [14] Y. H. Jung, B. Park, J. U. Kim, T.-I. Kim, *Adv. Mater.* **2019**, *31*, 1803637.
 [15] Y. Kim, A. Chortos, W. Xu, Y. Liu, J. Y. Oh, D. Son, J. Kang, A. M. Foudeh, C. Zhu, Y. Lee, S. Niu, J. Liu, R. Pfattner, Z. Bao, T. W. Lee, *Science* **2018**, *360*, 998.
 [16] Y. Zhang, T. H. Tao, *Adv. Funct. Mater.* **2020**, *30*, 2000381.
 [17] T. Yokota, P. Zalar, M. Kaltenbrunner, H. Jinno, N. Matsuhisa, H. Kitanosako, Y. Tachibana, W. Yukita, M. Koizumi, T. Someya, *Sci. Adv.* **2016**, *2*, e1501856.
 [18] T. Kim, J. S. Price, A. Grede, S. Lee, G. Choi, W. Guan, T. N. Jackson, N. C. Giebink, *Adv. Mater. Technol.* **2018**, *3*, 1800067.
 [19] C. Larson, B. Peele, S. Li, S. Robinson, M. Totaro, L. Beccai, B. Mazzolai, R. Shepherd, *Science* **2016**, *351*, 1071.
 [20] D. Son, J. Kang, O. Vardoulis, Y. Kim, N. Matsuhisa, J. Y. Oh, J. W. To, J. Mun, T. Katsumata, Y. Liu, A. F. McGuire, M. Krason, F. Molina-Lopez, J. Ham, U. Kraft, Y. Lee, Y. Yun, J. B. H. Tok, Z. Bao, *Nat. Nanotechnol.* **2018**, *13*, 1057.
 [21] Y. J. Tan, H. Godaba, G. Chen, S. T. M. Tan, G. Wan, G. Li, P. M. Lee, Y. Cai, S. Li, R. F. Shepherd, J. S. Ho, B. C. K. Tee, *Nat. Mater.* **2020**, *19*, 182.
 [22] Z. Zhang, L. Cui, X. Shi, X. Tian, D. Wang, C. Gu, E. Chen, X. Cheng, Y. Xu, Y. Hu, J. Zhang, L. Zhou, H. H. Fong, P. Ma, G. Jiang, X. Sun, B. Zhang, H. Peng, *Adv. Mater.* **2018**, *30*, 1800323.
 [23] X. Shi, X. Zhou, Y. Zhang, X. Xu, Z. Zhang, P. Liu, Y. Zuo, H. Peng, *J. Mater. Chem. C* **2018**, *6*, 12774.
 [24] J. Wang, C. Yan, K. J. Chee, P. S. Lee, *Adv. Mater.* **2015**, *27*, 2876.
 [25] G. Lee, M. Kong, D. Park, J. Park, U. Jeong, *Adv. Mater.* **2020**, *32*, 1907477.
 [26] Y. Zuo, X. Xu, X. Tao, X. Shi, X. Zhou, Z. Gao, X. Sun, H. Peng, *J. Mater. Chem. C* **2019**, *7*, 4020.
 [27] Y. Zhang, Y. Fang, J. Li, Q. Zhou, Y. Xiao, K. Zhang, B. Luo, J. Zhou, B. Hu, *ACS Appl. Mater. Interfaces* **2017**, *9*, 37493.
 [28] B. Zou, Y. Chen, Y. Liu, R. Xie, Q. Du, T. Zhang, Y. Shen, B. Zheng, S. Li, J. Wu, W. Zhang, W. Huang, X. Huang, F. Huo, *Adv. Sci.* **2019**, *6*, 1801283.
 [29] Y. Zhou, S. Cao, J. Wang, H. Zhu, J. Wang, S. Yang, X. Wang, D. Kong, *ACS Appl. Mater. Interfaces* **2018**, *10*, 44760.
 [30] R. E. Young, F. M. Mencher, *Science* **1980**, *208*, 1286.
 [31] J. S. Sparks, R. C. Schelly, W. L. Smith, M. P. Davis, D. Tchernov, V. A. Pieribone, D. F. Gruber, *PLoS One* **2014**, *9*, e83259.
 [32] J. W. Hastings, *J. Mol. Evol.* **1983**, *19*, 309.
 [33] S. M. Jeong, S. Song, H. Kim, K. Joo, H. Takezoe, *Adv. Funct. Mater.* **2016**, *26*, 4848.

- [34] S. M. Jeong, S. Song, S. K. Lee, N. Y. Ha, *Adv. Mater.* **2013**, *25*, 6194.
- [35] S. Zhang, R. J. W. Teo, H. Su, C. S. Tan, T. K. S. Wong, *Opt. Mater. Express* **2016**, *6*, 2879.
- [36] L. Bao, X. Xu, Y. Zuo, J. Zhang, F. Liu, Y. Yang, F. Xu, X. Sun, H. Peng, *Sci. Bull.* **2019**, *64*, 151.
- [37] M. Bredol, H. S. Dieckhoff, *Materials* **2010**, *3*, 1353.
- [38] S. Li, B. N. Peele, C. M. Larson, H. Zhao, R. F. Shepherd, *Adv. Mater.* **2016**, *28*, 9770.
- [39] J. X. Wang, C. Y. Yan, G. F. Cai, M. Q. Cui, A. L. S. Eh, P. S. Lee, *Adv. Mater.* **2016**, *28*, 4490.
- [40] Y. Zhou, C. Zhao, J. Wang, Y. Li, C. Li, H. Zhu, S. Feng, S. Cao, D. Kong, *ACS Mater. Lett.* **2019**, *1*, 511.
- [41] F. Stauffer, K. Tybrandt, *Adv. Mater.* **2016**, *28*, 7200.
- [42] R. Shanker, S. Cho, A. Choe, M. P. Kim, Z. Khan, S. Kang, H. Ko, *Adv. Funct. Mater.* **2019**, *29*, 1904377.
- [43] S. Abasi, M. Amani Tehran, M. D. Fairchild, *Color Res. Appl.* **2020**, *45*, 208.
- [44] B. Allieri, S. Peruzzi, L. Antonini, A. Speghini, M. Bettinelli, D. Consolini, G. Dotti, L. E. Depero, *J. Alloys Compd.* **2002**, *341*, 79.
- [45] J. Ibañez, E. Garcia, L. Gil, M. Mollar, B. Marí, *Displays* **2007**, *28*, 112.
- [46] M. Wong, L. Chen, G. Bai, L. Huang, J. Hao, *Adv. Mater.* **2017**, *29*, 1701945.
- [47] Z. Li, P. Liu, X. Ji, J. Gong, Y. Hu, W. Wu, X. Wang, H. Q. Peng, R. T. K. Kwok, J. W. Y. Lam, J. Lu, B. Z. Tang, *Adv. Mater.* **2020**, *32*, 1906493.
- [48] G. Isapour, M. Lattuada, *Adv. Mater.* **2018**, *30*, 1707069.
- [49] H. Kim, H. Lee, I. Ha, J. Jung, P. Won, H. Cho, J. Yeo, S. Hong, S. Han, J. Kwon, K. J. Cho, S. H. Ko, *Adv. Funct. Mater.* **2018**, *28*, 1801847.
- [50] Y. Wang, H. Cui, Q. Zhao, X. Du, *Matter* **2019**, *1*, 626.